Solar Phys (2010) 264: 81–91
DOI 10.1007/s11207-010-9573-9

Measurements of Filament Height in Hα and EUV 304 Å

Yan Xu · Ju Jing · Haimin Wang

Received: 8 December 2008 / Accepted: 7 May 2010 / Published online: 5 June 2010

Abstract In this study, we present the three-dimensional (3D) configuration of a filament observed by STEREO and the Global High Resolution H-alpha Network (GHN) in EUV 304 Å and Hα line center, respectively. This was the largest filament located close to the active region NOAA 10956 that produced a small B9.6 flare and two Coronal Mass Ejections (CMEs) on 19 May 2007. The 3D coordinates of multiple points traced along this filament were reconstructed by triangulation from two different aspect angles. The two STEREO (A and B) spacecraft had a separation angle α of 8.6 degree on 19 May 2007. The "true" heights of the filament were estimated using STEREO images in EUV 304 and Hα images, respectively. Our results show that EUV emission of the filament originates from higher locations than the Hα emission. We also compare the measured reconstructed heights of the filaments in EUV with those reported in previous studies.

Keywords Corona · Filament · Magnetic fields · Prominences · Ultraviolet

1. Introduction

Observation from two different perspective angles enables us to reconstruct the 3D configuration of solar features. Previous implementations of solar stereoscopy involved observations either from two satellites or from ground combined with space observations (see, *e.g.*, Kane *et al.*, 1998; Kane *et al.*, 1998; Caroubalos and Steinberg, 1974). For slowly evolving structures, many studies used the solar rotation as good approximation of parallax angles (*e.g.*, Aschwanden and Bastian, 1994a, 1994b; Aschwanden *et al.*, 1995, 1999, 2000; Batchelor, 1994; Brajša *et al.*, 2004). The twin STEREO spacecraft, which were launched on 2006 October 25 (Kaiser *et al.*, 2008) and the SECCHI suit of telescopes including the EUVI instrument onboard (Wuelser *et al.*, 2004; Howard *et al.*, 2008) provide strictly simultaneous observations of the Sun for the first time from two view points. Therefore, stereoscopy

Y. Xu (✉) · J. Jing · H. Wang
Space Weather Research Lab, Center for Solar-Terrestial Research, New Jersey Institute of Technology, 323 Martin Luther King Blvd., Newark, NJ 07102-1982, USA
e-mail: yx2@njit.edu

could be carried out for any solar features, regardless of its motion and internal variation. Feng *et al.* (2007) studied the 3D configuration of coronal magnetic loops. They developed a systematic scheme to locate identical loop pairs and reconstructed the 3D shape using stereoscopic reconstruction (Inhester, 2006) and magnetic extrapolation (see, *e.g.*, Wiegelmann, 2004; Wiegelmann *et al.*, 2005). Aschwanden *et al.* (2008) discussed the 3D triangulation and reconstruction method in general and published the IDL package with detailed instructions online. The geometrical principle used by them is similar to that used in other methods (see, *e.g.*, Feng *et al.*, 2007; Liewer *et al.*, 2009), but they track a coronal loop in image A (obtained by STEREO A) first and find the projected positions in image B (obtained by STEREO B) assuming a reasonable height range of the loop.

Beside coronal loops in the studies discussed above, filaments are other interesting solar features which are also good candidates for 3D reconstruction. They are referred to as prominences when observed close to the solar limb. Hα at 6563 Å and EUV line observations at He II 304 Å have always been used to observe filaments because of their suitable formation temperatures, *i.e.* $\sim$10 000 K for Hα and $\sim$80 000 K for EUV 304 (Wang *et al.*, 1998). Previously the height was measured either using observations of prominences close to the limb (Wang *et al.*, 1998) or indirectly estimated from their rotation rate (Rosa, 1996) for filaments on the solar disk. The former method is a direct measurement and the latter estimates the height by determining the projected width with the assumption that a filament is a thin plasma sheet. This method works well only for filaments with central meridian offsets ranging between 20 and 60 degrees (Rosa, 1996). This limitation was confirmed by Vršnak *et al.* (1999). Recently, Gissot *et al.* (2008) estimated the height of an erupting filament on 19 May 2007 in EUV 304 Å with a method called *Velociraptor* (Gissot *et al.*, 2003; Gissot and Hochedez, 2007). They estimated the height directly from simultaneously obtained EUVI images. Using the same data set, Liewer *et al.* (2009) studied the same erupting filament for a longer time period. Their result shows that this filament remained low in height until 11:30 UT and later erupted displaying a surge-like motion.

Since the method described by Aschwanden *et al.* (2008) is published as an open-source package, we adapted and modified their package for studying filaments in both Hα and EUV 304. We selected the largest filament close to the active region NOAA 10956 on 19 May 2007, which was also studied by Gissot *et al.* (2008) and Liewer *et al.* (2009). This active region produced a B9.6 flare around 12:50 UT. It was a complicated event involving a flare, a filament disappearance/eruption and also two CMEs. Several studies have been carried out to analyze this event from different aspects using SECCHI/STEREO data (see, *e.g.*, Li *et al.*, 2008; Long *et al.*, 2008; Veronig, Temmer, and Vršnak, 2008; Gopalswamy *et al.*, 2009). In addition to the He II images obtained from STEREO, we included Hα images obtained from the Global High Resolution Hα Network (GHN), which show a better contrast of filaments. We present our stereoscopic reconstruction for both EUV 304 and Hα filaments in this paper and compare the reconstructed heights with those reported in previous studies (see, *e.g.*, Gissot *et al.*, 2008; Liewer *et al.*, 2009; Wang *et al.*, 1998).

2. Observation and Data Reduction

The EUV 304 Å images analyzed in this paper were obtained by EUVI instrument on board STEREO (Wuelser *et al.*, 2004). The pixel resolution of the EUVI images is about 1.6″ and the field-of-view (FOV) is up to 1.7 solar radius. The separation angle α_{sep} between STEREO

A and B was about 8.6° on 19 May 2007. We follow the procedure described by Aschwanden *et al.* (2008) to reconstruct the 3D coordinates of the filament in EUV 304 Å. The data processing includes calibration, co-alignment, intensity normalization, feature tracing, coordinate transfer, stereoscopic 3D reconstruction and curvilinear fitting. The first three steps were done automatically by the STEREO package in the SolarSoftWare (SSW). However, the tracing of the filament was done manually because it is more reliable than the currently existing automated methods (Aschwanden *et al.*, 2008). We applied this 3D reconstruction technique to all the EUV 304 image pairs obtained on 19 May 2007 before the eruption, *e.g.* from 00:11:45 UT to 12:51:45 UT. Unlike coronal loops, filaments are extended sources with tens of arcseconds in radial direction. Even if we assume that filaments have a perfect symmetric shape, it is hard to find single conjugate points in image A and B representing the same point on the 3D surface of filaments. Therefore, we study a filament as a whole according to its shape. Since the filament analyzed here shows a 'bow-shaped' structure, all spline points are selected along several loops. After tracing out the selected points in both images A and B, the program calculates the corresponding epipolar positions and estimates the height of the filament at those points.

The full-disk Hα filtergrams used in this paper were obtained by Kanzelhöhe Solar Observatory, Austria, which is one of the stations of the GHN. The Hα high resolution data were obtained with large-format of pixels using a $2k \times 2k$, 14 bit digital camera. The image scale is approximately $1''$ pixel^{-1} and time cadence is up to one minute. The raw image was corrected for dark current, flat field and was subsequently rotated by P-angle. These images were further processed as per the steps discussed above for the EUV images. The only difference is that the parallax angle for the Hα data is determined by position difference due to solar rotation. The time interval is set to be several hours. Within such a period, the filament did not change much and the rotation angle is large enough for stereoscopy. For this particular event, we selected a time interval of about 18 hours, which corresponds to a rotation angle of nine degrees in accordance with the separation angle of the STEREO images in EUV 304. The Sun not only rotates differentially with latitude but its rotation velocity also varies vertically from the photosphere to corona. Photospheric differential rotation could be measured either by tracing sunspots (Beck, 2000) or by analyzing Doppler signals (Howard, Boyden, and Labonte, 1980). While for the chromosphere and above, the rotation rate could be determined either by tracing filaments (Brajsa *et al.*, 1991; Vršnak *et al.*, 1999) or by measuring the displacements of features using cross-correlation technique (Steinegger *et al.*, 2001). The results from both the methods matched very well. Therefore, we choose to use the synodic rotation rate of 13.3044 ± 0.0003 degree/day (see Table 2 in Steinegger *et al.* (2001)). Another method is to use the 'get_sun' function in SSW to obtain the Carrington rotation number at each time and use the difference to derive the rotation angle. This method uses a uniform rotation speed of the Sun and works fine only for features close to the solar equator. Since the filament studied in this paper is located at lower latitudes, the difference of rotation angles calculated using the above two methods is less than one percent.

Due to the seeing variation, the image quality varies from image to image. The program also provides a tool to calculate the offset in x and y directions between two images in one stereoscopic pair. The results are used to determine how good the co-alignments are. Table 1 lists these offsets for different Hα image pairs as well as the five EUV image pairs. Hα image pairs 8 and 10 have relatively smaller offsets and are selected for 3D reconstruction. The observing time of each image and the equivalent separation angle of each pair are also listed in Table 1.

Table 1 List of image pairs.

Number	Time 19 May 2007	d*x* (pix)	d*y* (pix)	Roll (deg)	Sep. Angle (deg)
1	EUV 00:21:45 (A and B)	-1.04 ± 0.31	0.67 ± 0.13	0.03 ± 0.05	8.56
2	EUV 03:21:45 (A and B)	-0.86 ± 0.41	0.49 ± 0.27	0.03 ± 0.05	8.58
3	EUV 06:21:45 (A and B)	-1.08 ± 0.56	0.55 ± 0.21	0.03 ± 0.05	8.60
4	EUV 12:21:45 (A and B)	-0.85 ± 0.47	0.86 ± 0.68	0.02 ± 0.05	8.64
5	EUV 12:41:45 (A and B)	-1.13 ± 0.76	1.29 ± 1.32	0.01 ± 0.05	8.64
6	Hα image A,[a] 08:17:03	-1.95 ± 0.15	5.78 ± 5.43	0.42 ± 0.05	9.86
7	Hα image A,[a] 08:27:03	-2.01 ± 0.13	3.67 ± 0.74	0.22 ± 0.05	9.95
8	Hα image A,[a] 08:47:03	0.20 ± 0.10	-0.34 ± 1.14	0.08 ± 0.05	10.14
9	Hα image A,[a] 09:17:03	-0.69 ± 0.02	5.18 ± 2.43	-0.13 ± 0.05	10.41
10	Hα image A,[a] 09:07:03	-1.28 ± 0.10	0.70 ± 0.91	0.23 ± 0.05	10.32

[a]This image was taken at 14:29:49 UT on 18 May 2007.

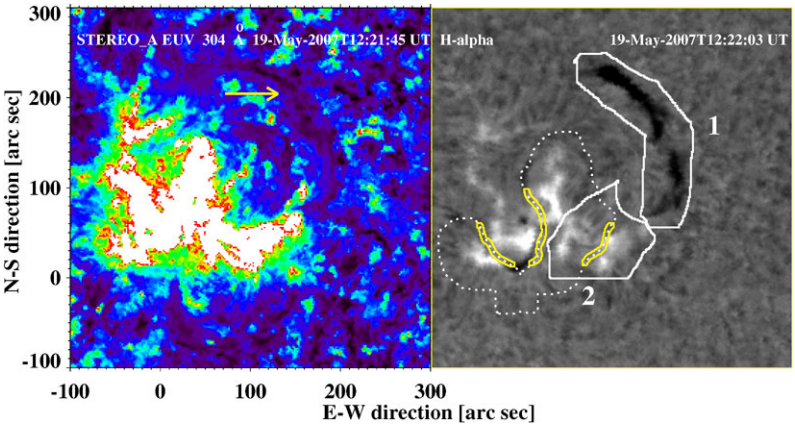

Figure 1 Images of active region NOAA 10956 on 19 May 2007. Left: EUV 304 Å from EUVI/STEREO A at 12:21:45 UT, the dark feature pointed by the yellow arrow is the filament studied in this paper; Right: Hα image taken by Kanzelhöhe Solar Observatory at 12:22:03 UT, superimposed with magnetic neutral lines as dotted white lines. In order to compare with EUVI image, both Hα and MDI magnetogram have been rotated by 9.056 degrees, which is the angle between the ecliptic plane and the spacecraft A – B plane. The yellow portions of neutral lines indicate areas with a strong magnetic gradient. Area 1 enclosed by white line indicates the filament region and Area 2 covers the flare region.

3. Analysis and Results

Figure 1 shows the images obtained in EUV 304 Å (left) at 12:21:45 UT and Hα (right) at 12:22:03 UT. The FOV is about 400 × 400 arcseconds. In the Hα image (right), two groups of filaments could be identified, several small filaments are close to the active region center (sunspot) and one large filament is suspended far away to the northwest. Due to the strong emission around the sunspot region, the small filaments are invisible in EUV 304 Å; only the large filament could be observed both in Hα and EUV. The spatial correlation of this filament in these two wavelengths is very good as shown in Figure 4c of Li *et al.* (2008).

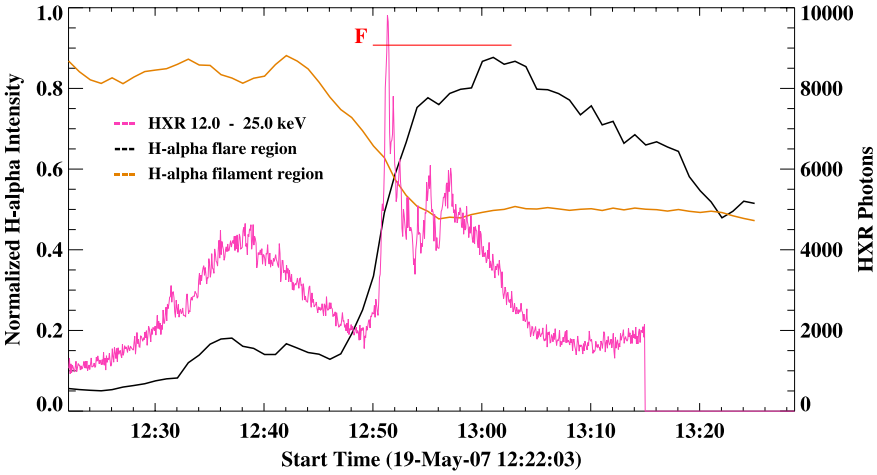

Figure 2 RHESSI HXR light curve in the energy ranges of 12 – 25 keV (Pink) and Hα light curves of the flare region (black) and filament area (brown). The Hα curves are normalized to their maximum (black)/minimum (brown). The flare period is tagged with 'F' on the top.

The white dotted lines in the Hα image indicate the magnetic neutral lines derived from MDI magnetogram. Three strong neutral lines are marked by thick yellow curves, corresponding to the highest magnetic gradient. All filaments are aligned with strong magnetic neutral lines very well except the large filament (Area 1 in right panel of Figure 1), which was a dynamic filament and eventually erupted (Bone *et al.*, 2009). The filament eruption was also associated with a B9.6 flare and a CME. In order to better understand the interaction between filament eruption and flare occurrence, the temporal evolution of both the phenomena are investigated. Hard X-ray (HXR) and Hα light curves are plotted in Figure 2. The pink curve is HXR of energy band 12 – 25 keV. The black and brown curves are the time profiles of Hα intensity in filament and flare regions, which are marked by white lines 1 and 2 in Figure 1. The units of Hα plots are normalized to the maximum values for flare areas and to the minimum value for filament areas, respectively. Both the Hα light curves are smoothed with two-point average. Large values of the black curve suggest high intensities of the flare region. For the filament region, the decrease in the value of intensity suggests disappearance of the filament. Starting from 12:30 UT, the intensities in HXR and Hα flare region increase simultaneously indicating a heating process (Bone *et al.*, 2009), although this emission is of insufficient magnitude to be classified as a flare. At the same time, a perturbation in the filament's light curve is seen, which is also observed in the movie (http://solar.njit.edu/~yxu/hamovie_20070519/ha.avi). Therefore, we selected images taken before 12:30 UT for 3D reconstructions to ensure that the shape of the filament remains the same in the Hα images.

3.1. Stereoscopy in EUV 304

The EUV image pair taken at 12:21:45 UT is used for the 3D construction of this filament. The left image in Figure 3 shows the original intensity map from STEREO A with partial FOV covering the active region and the filament being reconstructed in this study. The preprocessing steps for the 3D reconstruction include calibration, co-centering, rebinning of both images A and B and rotation of image B to the same parameters as image A (As-

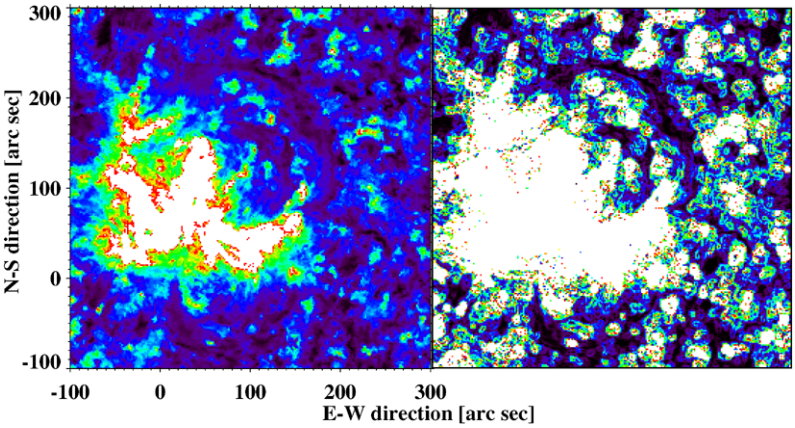

Figure 3 Original EUV 304 image (left) *vs.* contrast enhanced image (right).

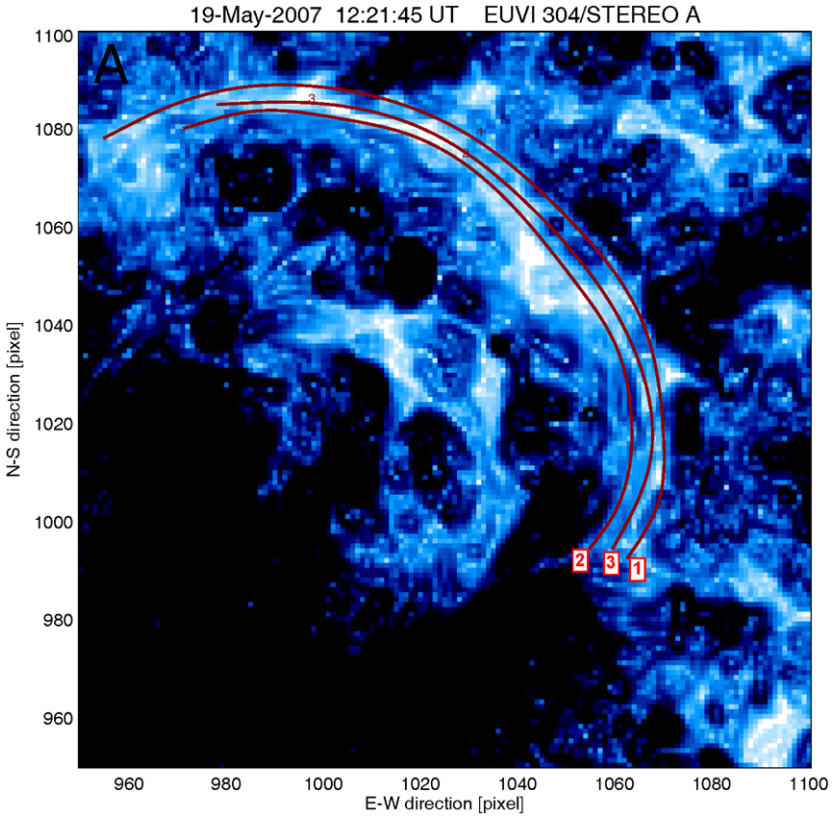

Figure 4 Spline curves represent different parts of the filament overlaid on *negative* EUV 304 image from STEREO A. Curves 1 and 2 outline the filament boundaries and Curve 3 traces the central part along the filament.

chwanden *et al.*, 2008). After these steps, we convert the intensity map to a contrast map by:

$$c = \frac{I - b}{b}, \tag{1}$$

where c and I denote contrast and intensity maps, respectively, where b is background (quiet sun area close to the active region) obtained from the intensity map. The Sobel function is then applied to the contrast image to enhance the boundaries of the filament, which is shown in Figure 3 (right panel). The projected geometric shape of the filament could be further decomposed to a bundle of "parallel" curvilinear futures, for instance, two boundaries and cross-sectional centroid of the filament. As shown in Figure 4, we choose to determine the heights of the points with peak contrasts (red Curve 3 in the middle) along the filament and outer (red Curve 1) and inner boundaries (red Curve 2) in the 2D image. Note that the background image is actually *imageB – imageA* and the contrast is inversed from the original image A. Therefore the filament shows a positive contrast (white color) in this figure. Along each of these three curves, multiple spline points are selected in both images A and B. The IDL program connects these points by applying high resolution 2D spline interpolation. The interpolation process helps to reduce the redundancy and visual input error (Aschwanden *et al.*, 2008). For each interpolated point, its 3D coordinates are reconstructed, in principle, by measuring the difference of its projected positions on images A and B. Consequently the heights of multiple spans (Curves 1, 2 and 3) along the filament are calculated. The results

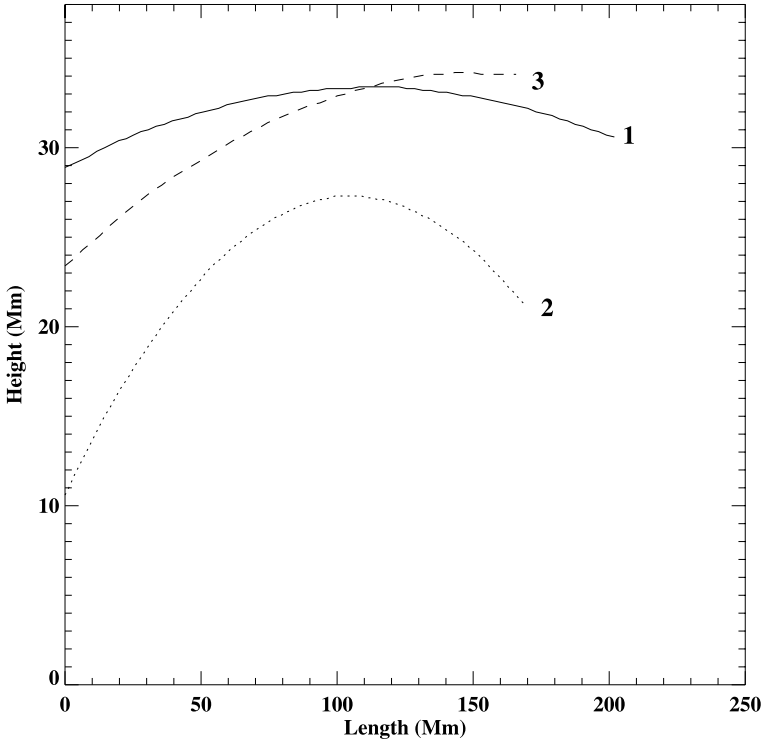

Figure 5 Estimated true heights measured from EUV 304 images as functions of filament length shown in Figure 4 along spline Curves 1, 2 and 3.

are plotted in Figure 5. The solid line shows the height variation of Curve 1 in Figure 4, while dotted and dashed plots are for Curves 2 and 3. For each curve, the first spline point at the lower-right end of the filament was defined as the *original point*. Therefore, the x-axis represents the length along the filament from the *original point*. It shows that the heights along Curves 1 and 3 have maxima of 33.4 ± 4.5 and 34.2 ± 4.7 Mm, respectively. Curve 2 has a height of 27.3 ± 5.2 Mm, which is systematically lower than the heights computed at the ridge and upper boundary of the filament. Note that Curve 2 is the inner boundary, which is closer to the solar disk center, and therefore should represent the lowest part of this filament.

3.2. Stereoscopy in Hα

The process of 3D reconstruction for Hα filament is similar to that described in Section 2 for a filament observed in He 304. The main advantage of the GHN Hα data is the long duration of continuous observations providing multiple observing angles and stereo-image pairs with different separation angles. The 3D reconstruction is carried out for image pairs 8 and 10 (see Table 1) and the reconstructed height and length of the filament are plotted in Figure 6. Since the width of the filament in Hα is smaller than in EUV 304, we selected points on the filament in Hα for reconstruction along the central part, which corresponds to Curve 3 in EUV 304. It is found that the maximum height in Hα of this filament ranges between 24 to 31 Mm. This reconstructed height is lower than that measured in EUV 304. The difference in reconstructed heights as measured in Hα and EUV is consistent with previous results

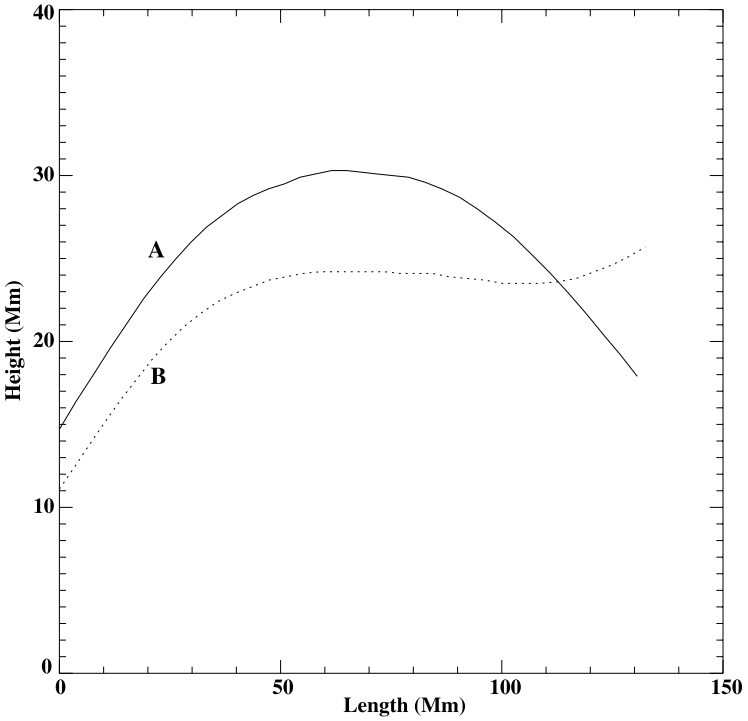

Figure 6 Estimated true heights measured from Hα image pairs 8 (solid Curve A) and 10 (dotted Curve B). The observing time and corresponding parameters of each image pair are listed in Table 1.

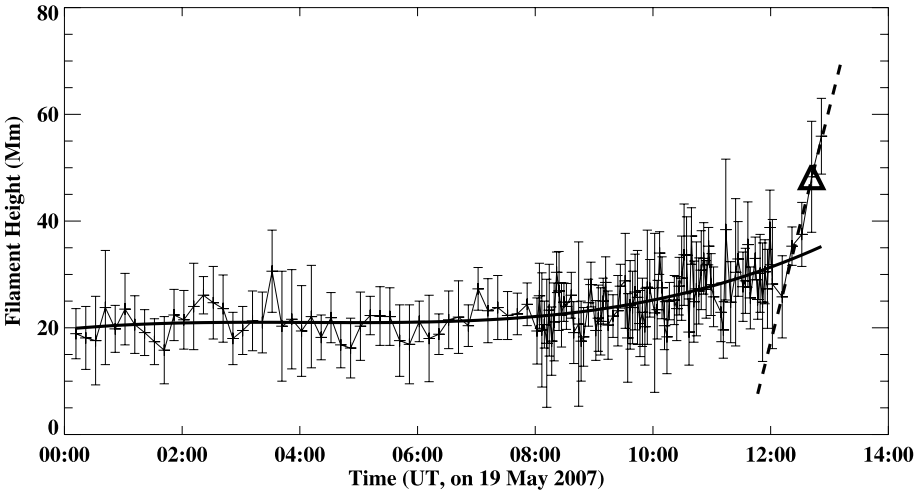

Figure 7 Height measurements of the filament in EUV 304 from 00:11:45 UT to 12:51:45 UT. The dense data points after 08:00 UT indicates a higher observing cadence. The big triangle shows the data point at 12:41:45 UT. The thick solid curve represents the third order fitting of the height variation as a function of time before 11:54:15 UT. The dashed fitting is a linear fit after 12:11:45 UT. The intersection point at 12:21 UT separates the gradual-rising phase and the erupting phase.

by Wang *et al.* (1998). They measured the projected heights of a prominence observed on 26 August 1997 and 13 January 1998 and concluded that prominences appeared higher in EUV 304 than in Hα due to their higher temperature. The reconstructed 3D configuration obtained from two image pairs in Hα show similar shapes, but the measured heights differ by 7 Mm, which is approximately 29% of the 24 Mm, the lower limit of the height range. Multiple measurements show that this difference is not due to measurement errors. One possibility for this difference in height could be that it is due to a real change in filament height in a time span of 18 hours. In fact, Liewer *et al.* (2009) show that the height varies by a small amount before the flare occurred.

In order to confirm the variation of the height of the filament, all the EUV image pairs taken before the eruption were used for 3D reconstruction. As shown in Figure 7, we measured the height of the filament (with error estimation) from 00:11:45 UT to 12:51:45 UT in EUV 304. The results show that the filament height changes even before the eruption. Although the height increase slowly, it becomes more obvious after 08:00 UT. Since the later images in both reconstructed Hα pairs were taken after 08:00 UT, the reconstruction in Hα could be affected and results in larger uncertainties than the EUV 3D reconstructions.

4. Discussion and Conclusion

We have presented 3D reconstruction of a filament on solar disk observed in EUV 304 Å and Hα. Our result shows that the maximum height of this filament is about 34 Mm as measured from EUV 304 images, which is slightly higher than 31 Mm, obtained from the Hα images. Wang *et al.* (1998) studied a prominence observed on 13 January 1998 in EUV 304 and Hα. They found that Hα and EUV emission originate from the lower and higher part of the prominence, respectively, indicating a hot-cool configuration defined by Zirin

(1988). Our results also confirm that filaments observed on the solar disk are higher in EUV 304 than in Hα.

Gissot *et al.* (2008) and Liewer *et al.* (2009) analyzed the same filament in EUV 304 using different techniques. Their results show the height was about 44 Mm at 12:41:25 UT. Our method yields a similar result of 48.2 ± 10.4 Mm. This result is highlighted using a triangle in Figure 7. In addition, we applied our method to the entire EUVI data set from 00:11:45 UT to 12:51:45 UT, when the filament started to erupt. Two phases of upward motions could be identified. The first phase is a slow-rising phase that started at about 08:00 UT. The higher observing cadence after 08:00 UT also shows the increase in height more clearly. The second phase was the actual eruptive phase. We fitted the last five points with a linear function. The result is plotted as a dashed line in Figure 7. The intersection point at 12:21:00 UT indicates the change over of the two phases of eruption. By neglecting weak perturbation of the filament prior to 08:00 UT, we fit the heights in a four-hour time interval starting 08:00 UT with a constant acceleration. The result shows that the filament has an upward acceleration of 9.2 ± 0.7 cm s^{-2}, which is consistent with the result of Joshi and Srivastava (2007), who found an acceleration range of $4-12$ cm s^{-2} for prominences observed in EUV 304. Sterling and Moore (2005) reported a constant speed of an eruptive filament observed on 11 July 1998. However, their result is based on a study of a very short period of 10 minutes. In a much longer time interval, *e.g.*, four hours in this study, the slow-acceleration phase becomes conspicuous. In the fast-rise phase, the rising speed of this filament is 12.2 ± 1.2 km s^{-1}. This speed is very slow compared with the previous results (Sterling and Moore, 2005; Joshi and Srivastava, 2007). However, we only measure the very beginning stage of the fast-rise phase and the maximum height was below 60 Mm. Taking an approximate value of acceleration in this phase, for instance $\sim$0.6 km s^{-2} as found by Sterling and Moore (2005), the eruption speed will attain a value of several hundreds km s^{-1}.

As the filament height varied before the eruption, this is probably why the result of Hα analysis has a significantly large uncertainty. Therefore our method is sensitive to the height variation during a certain period. This indicates that the filament on 19 May 2009 is not a perfect candidate for stereoscopy in Hα. We plan to apply our method to stable filaments so as to compare the results of stereoscopic reconstruction using EUV 304 and Hα images.

Acknowledgements The authors would thank Dr. Markus Aschwanden for providing the 3D reconstruction code and valuable discussion. The authors sincerely thank the anonymous referee for his/her suggestions to improve this paper. We also thank Drs. Yan Li and Paulett Liewer for their comments and suggestions. The Global High Resolution Ha Network is supported by NSF under grant ATM-0839216. This work is supported by NASA under grants NNX08-AJ23G and NNX08-AQ90G. JJ was supported by NSF under grant ATM 09-36665 and ATM 07-16950. The STEREO/SECCHI data used here were produced by an international consortium of the Naval Research Laboratory (USA), Lockheed Martin Solar and Astrophysics Lab (USA), NASA Goddard Space Flight Center (USA), Rutherford Appleton Laboratory (UK), University of Birmingham (UK), Max-Planck-Institut for Solar System Research (Germany), Centre Spatiale de Liège (Belgium), Institut d'Optique Thorique et Appliquée (France), and Institut d'Astrophysique Spatiale (France). The USA institutions were funded by NASA, the UK institutions by the Science & Technology Facility Council (which used to be the Particle Physics and Astronomy Research Council, PPARC), the German institutions by Deutsches Zentrum für Luftund Raumfahrt e.V. (DLR), the Belgian institutions by Belgian Science Policy Office, and the French institutions by Centre National d'Etudes Spatiales (CNES) and the Centre National de la Recherche Scientifique (CNRS). The NRL effort was also supported by the USAF Space Test Program and the Office of Naval Research.

References

Aschwanden, M.J., Bastian, T.S.: 1994a, *Astrophys. J.* **426**, 425. doi:10.1086/174078.
Aschwanden, M.J., Bastian, T.S.: 1994b, *Astrophys. J.* **426**, 434. doi:10.1086/174079.

Aschwanden, M.J., Lim, J., Gary, D.E., Klimchuk, J.A.: 1995, *Astrophys. J.* **454**, 512. doi:10.1086/176502.
Aschwanden, M.J., Newmark, J.S., Delaboudinière, J.P., Neupert, W.M., Klimchuk, J.A., Gary, G.A., Portier-Fozzani, F., Zucker, A.: 1999, *Astrophys. J.* **515**, 842. doi:10.1086/307036.
Aschwanden, M.J., Alexander, D., Hurlburt, N., Newmark, J.S., Neupert, W.M., Klimchuk, J.A., Gary, G.A.: 2000, *Astrophys. J.* **531**, 1129. doi:10.1086/308483.
Aschwanden, M.J., Wülser, J.P., Nitta, N.V., Lemen, J.R.: 2008, *Astrophys. J.* **679**, 827. doi:10.1086/529542.
Batchelor, D.: 1994, *Solar Phys.* **155**, 57. doi:10.1007/BF00670730.
Beck, J.G.: 2000, *Solar Phys.* **191**, 47.
Bone, L.A., van Driel-Gesztelyi, L., Culhane, J.L., Aulanier, G., Liewer, P.: 2009, *Solar Phys.* **259**, 31. doi:10.1007/s11207-009-9427-5.
Brajsa, R., Vrsnak, B., Ruzdjak, V., Schroll, A., Pohjolainen, S.: 1991, *Solar Phys.* **133**, 195. doi:10.1007/BF00149885.
Brajša, R., Wöhl, H., Vršnak, B., Ruždjak, V., Clette, F., Hochedez, J.F., Roša, D.: 2004, *Astron. Astrophys.* **414**, 707. doi:10.1051/0004-6361:20034082.
Caroubalos, C., Steinberg, J.L.: 1974, *Astron. Astrophys.* **32**, 245.
Feng, L., Inhester, B., Solanki, S.K., Wiegelmann, T., Podlipnik, B., Howard, R.A., Wuelser, J.P.: 2007, *Astrophys. J. Lett.* **671**, 205. doi:10.1086/525525.
Gissot, S.F., Hochedez, J.F.: 2007, *Astron. Astrophys.* **464**, 1107. doi:10.1051/0004-6361:20065553.
Gissot, S.F., Hochedez, J.F., Dibos, F., Brajša, R., Jacques, L., Berghmans, D., Zhukov, A., Clette, F., Wöhl, H., Antoine, J.P.: 2003, *Extracting the Apparent Motion from Two Successive EIT Images* **535**, 853.
Gissot, S.F., Hochedez, J.F., Chainais, P., Antoine, J.P.: 2008, *Solar Phys.* **252**, 397. doi:10.1007/s11207-008-9270-0.
Gopalswamy, N., Yashiro, S., Temmer, M., Davila, J., Thompson, W.T., Jones, S., McAteer, R.T.J., Wuelser, J.P., Freeland, S., Howard, R.A.: 2009, *Astrophys. J. Lett.* **691**, 123. doi:10.1088/0004-637X/691/2/L123.
Howard, R., Boyden, J.E., Labonte, B.J.: 1980, *Solar Phys.* **66**, 167. doi:10.1007/BF00150527.
Howard, R.A., Moses, J.D., Vourlidas, A., Newmark, J.S., Socker, D.G., Plunkett, S.P., Korendyke, C.M., Cook, J.W., Hurley, A., Davila, J.M., *et al.*: 2008, *Space Sci. Rev.* **136**, 67. doi:10.1007/s11214-008-9341-4.
Inhester, B.: 2006, ArXiv:astro-ph/0612649 Astrophysics e-prints.
Joshi, V., Srivastava, N.: 2007, *Bull. Astron. Soc. India* **35**, 447.
Kaiser, M.L., Kucera, T.A., Davila, J.M., St. Cyr, O.C., Guhathakurta, M., Christian, E.: 2008, *Space Sci. Rev.* **136**, 5. doi:10.1007/s11214-007-9277-0.
Kane, S.R., Hurley, K., McTiernan, J.M., Boer, M., Niel, M., Kosugi, T., Yoshimori, M.: 1998, *Astrophys. J.* **500**, 1003. doi:10.1086/305738.
Li, Y., Lynch, B.J., Stenborg, G., Luhmann, J.G., Huttunen, K.E.J., Welsch, B.T., Liewer, P.C., Vourlidas, A.: 2008, *Astrophys. J. Lett.* **681**, 37. doi:10.1086/590340.
Liewer, P.C., de Jong, E.M., Hall, J.R., Howard, R.A., Thompson, W.T., Culhane, J.L., Bone, L., van Driel-Gesztelyi, L.: 2009, *Solar Phys.* **256**, 57. doi:10.1007/s11207-009-9363-4.
Long, D.M., Gallagher, P.T., McAteer, R.T.J., Bloomfield, D.S.: 2008, *Astrophys. J. Lett.* **680**, 81. doi:10.1086/589742.
Rosa, D.: 1996, *Hvar Obs. Bull.* **20**, 41.
Steinegger, M., Denker, C., Goode, P.R., Marquette, W.H., Varsik, J., Wang, H., Otruba, W., Freislich, H., Hanslmeier, A., Luo, G., Chen, D., Zhang, Q.: 2001, *The New Global High-Resolution* Hα *Network: Preliminary Results on the Chromospheric Differential Rotation* **464**, 315.
Sterling, A.C., Moore, R.L.: 2005, *Astrophys. J.* **630**, 1148. doi:10.1086/432044.
Veronig, A.M., Temmer, M., Vršnak, B.: 2008, *Astrophys. J. Lett.* **681**, 113. doi:10.1086/590493.
Vršnak, B., Rošd, A., Božić, H., Brajša, R., Ruždjak, V., Schroll, A., Wöhl, H.: 1999, *Solar Phys.* **185**, 207.
Wang, H., Chae, J., Gurman, J.B., Kucera, T.A.: 1998, *Solar Phys.* **183**, 91.
Wiegelmann, T.: 2004, *Solar Phys.* **219**, 87. doi:10.1023/B:SOLA.0000021799.39465.36.
Wiegelmann, T., Inhester, B., Lagg, A., Solanki, S.K.: 2005, *Solar Phys.* **228**, 67. doi:10.1007/s11207-005-2511-6.
Wuelser, J.P., Lemen, J.R., Tarbell, T.D., Wolfson, C.J., Cannon, J.C., Carpenter, B.A., Duncan, D.W., Gradwohl, G.S., Meyer, S.B., Moore, A.S., et al.: 2004, *Presented at the Society of Photo-Optical Instrumentation Engineers (SPIE) Conference* **5171**, 111. doi:10.1117/12.506877. http://spiedl.aip.org/getabs/servlet/GetabsServlet?prog=normal&id=PSISDG005171000001000111000001&idtype=cvips&gifs=yes.
Zirin, H.: 1988, *Astrophysics of the Sun*, Cambridge University Press, Cambridge, 440 p.